

Research Article

Open Access



Improved thermoelectric performance in n-type flexible $\text{Bi}_2\text{Se}_{3+x}$ /PVDF composite films

Qi Zou^{1,2,#}, Hongjing Shang^{1,2,#}, Daxing Huang^{1,2}, Taiguang Li^{1,2}, Bowei Xie^{1,2}, Hongwei Gu^{1,2}, Fazhu Ding^{1,2}

¹Key Laboratory of Applied Superconductivity and Institute of Electrical Engineering, Chinese Academy of Sciences, Beijing 100190, China.

²University of Chinese Academy of Sciences, Beijing 100049, China.

#Authors contributed equally.

Correspondence to: Prof. Fazhu Ding, Key Laboratory of Applied Superconductivity and Institute of Electrical Engineering, Chinese Academy of Sciences, 6 Beiertiao Road Haidian District, Beijing 100190, China. E-mail: dingfazhu@mail.iee.ac.cn

How to cite this article: Zou Q, Shang H, Huang D, Li T, Xie B, Gu H, Ding F. Improved thermoelectric performance in n-type flexible $\text{Bi}_2\text{Se}_{3+x}$ /PVDF composite films. *Soft Sci* 2021;1:2. <http://dx.doi.org/10.20517/ss.2021.04>

Received: 9 Jun 2021 **First Decision:** 16 Jun 2021 **Revised:** 29 Jun 2021 **Accepted:** 1 Jul 2021 **First online:** 1 Jul 2021

Academic Editor: Zhifeng Ren **Copy Editor:** Xi-Jun Chen **Production Editor:** Xi-Jun Chen

Abstract

Bismuth selenide materials (Bi_2Se_3) have high performance around room temperature, demonstrating potential in thermoelectric applications. Presently, most vacuum preparation techniques used to fabricate the film materials, such as magnetron sputtering and molecular beam epitaxy, usually require complex and expensive equipment. This limits the practical applications of flexible thermoelectric films. Here, we prepared $\text{Bi}_2\text{Se}_{3+x}$ nanoplate/polyvinylidene fluoride composite films with good flexibility using a facile chemical reaction method. Their thermoelectric performance and microstructures were systematically studied. The composite films exhibit a highly preferred orientation along (015). The carrier concentration and mobility were optimized by adding excessive element Se, eventually leading to an improvement in thermoelectric performance. The optimized power factor is $5.2 \mu\text{W}/\text{K}^2\text{m}$ at 300 K. Furthermore, the performance remains stable after 2500 bending cycles at a radius of 1 cm, suggesting promising applications in wearable/portable electronics.

Keywords: Bi_2Se_3 , flexible, thermoelectric films, heterostructure

INTRODUCTION

Recently, wearable/portable electronic devices are ubiquitous, bringing great convenience to our lives^[1-3]. However, they are usually dependent on the power from traditional chemical batteries with a finite lifetime



© The Author(s) 2021. **Open Access** This article is licensed under a Creative Commons Attribution 4.0 International License (<https://creativecommons.org/licenses/by/4.0/>), which permits unrestricted use, sharing, adaptation, distribution and reproduction in any medium or format, for any purpose, even commercially, as long as you give appropriate credit to the original author(s) and the source, provide a link to the Creative Commons license, and indicate if changes were made.



and requiring periodic recharging, thus limiting their further popularity^[4-6]. Thermoelectric materials, as one of the most competitive energy materials, can generate electricity from heat and realize the direct conversion between heat and electricity, showing a good potential in flexible electronics^[7-10]. Generally, the energy conversion efficiency of thermoelectric modules depends on the dimensionless thermoelectric figure of merit: zT , $zT = S^2\sigma T/\kappa$, where S is the Seebeck coefficient, σ is the electrical conductivity, κ is the thermal conductivity, T is the absolute temperature, and $S^2\sigma$ is the power factor^[11-13].

Bi_2Se_3 is a type of V_2VI_3 semiconductor material with a layered crystal structure, which exhibits excellent thermoelectric performance around room temperature^[14]. With the rapid development of wearable/portable electronics, thermoelectric films considering Bi_2Te_3 -based compounds have also been a hot area of research in recent years^[15,16]. Currently, there are many methods to fabricate the films, including top-down and bottom-up processes^[17]. Top-down processes use mechanical peeling or liquid phase peeling from the block to the sheet structure^[18]. Ambrosi *et al.*^[19] proposed a simple and rapid electrochemical approach to exfoliate natural Bi_2Se_3 and Bi_2Te_3 crystals in aqueous media to obtain single/few-layer nanoplates. However, this has a limitation on the dimension of the exfoliation materials, which also lacks good stability. Thus, it is challenging to obtain large-area films^[20,21]. On the other hand, classic bottom-up methods include chemical vapor deposition^[22], magnetron sputtering^[23,24], molecular beam epitaxy^[25], *etc.* These methods usually require high vacuum or complex equipment, largely limiting the practical applications. For example, thin films of $\text{Bi}_2\text{Te}_{2.7}\text{Se}_{0.3}$ were deposited on a SiO_2 -coated silicon (SiO_2/Si) substrate using a pulsed laser deposition system^[26], where the base pressure of 3.8×10^{-6} Torr and preheating temperature in the range of 20-800 °C are required. Fortunately, the chemical solution method can avoid this limitation as well as make it easier to prepare large-area films^[27]. Masood *et al.*^[28] used hydrazine hydrate to realize a redox reaction and synthesized Bi_2Te_3 nano-sticks.

In this study, we adopted a facile chemical solution method to prepare flexible $\text{Bi}_2\text{Se}_{3+x}/\text{PVDF}$ composite films. The reaction equipment is easy to assemble. It is emphasized that this chemical solution method is different from the previous reports^[29,30], where the reaction system ensures an inert atmosphere by circulating high-purity nitrogen. Ethylene glycol (EG) is used as a reducing agent, which is less toxic and safer than hydrazine hydrate. The whole process happens under the protection of high-purity nitrogen (N_2). PVDF is used to buffer the deformation and protect the matrix materials from destruction; it also regulates the thermoelectric performance by introducing organic-inorganic interfaces. Besides, the thickness and area of the flexible $\text{Bi}_2\text{Se}_{3+x}/\text{PVDF}$ composite films can be effectively adjusted by controlling the solution concentration and the substrate size. The composite films show a good flexibility and an improved thermoelectric performance, achieving a power factor of $5.2 \mu\text{W}/\text{K}^2\text{m}$ at 300 K.

EXPERIMENTAL

$\text{Bi}_2\text{Se}_{3+x}/\text{PVDF}$ thermoelectric films were prepared by the chemical solution method. The whole reaction process is shown in Figure 1A. Firstly, according to the chemical composition of the $\text{Bi}_2\text{Se}_{3+x}/\text{PVDF}$ thermoelectric films ($x = 0, 0.2, 0.3, 0.4$), analytically pure sodium selenite (Na_2SeO_3 , 99%, SIGMA-ALDRICH), bismuth nitrate [$\text{Bi}(\text{NO}_3)_3$, 98.0%, SIGMA], and ethylene glycol (EG, 99+%, Alfa Aesar) were mixed in a three-necked flask. High-purity nitrogen (N_2) was circulated in the reaction device for 20 min at a high speed to remove the air, ensuring an inert atmosphere. Then, the raw materials were reacted at 200 °C for 5 h to obtain $\text{Bi}_2\text{Se}_{3+x}$ powder. After the solution cooled to room temperature, the powder was precipitated using ethanol. The obtained pure $\text{Bi}_2\text{Se}_{3+x}$ powder and polyvinylidene fluoride powder (PVDF, ALDRICH) (2:1 ratio) were dissolved in dimethylformamide (DMF), obtaining a homogeneous suspension by ultrasound for 3 h. Finally, dripping the suspension on glass substrates and baking at 80 °C for 10-12 h achieved the composite films.

Ethylene glycol shows strong reducibility above 185 °C^[29,31], which can reduce the Se element from Se^{4+} to Se or Se^{2-} . Then, it can be reacted with Bi^{3+} to obtain Bi_2Se_3 nanoplates, as shown in Equations (2.1)-(2.3).

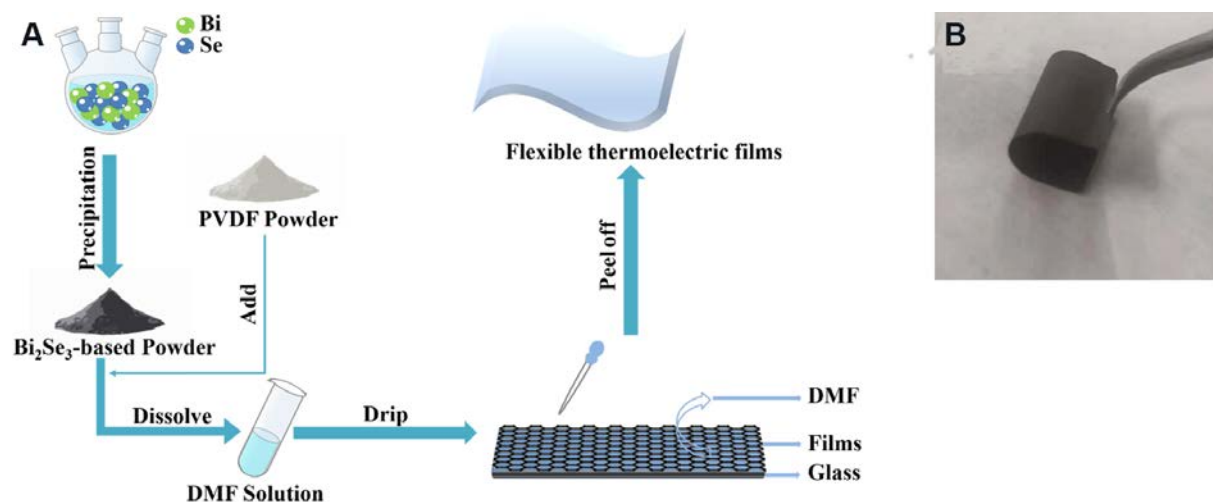


Figure 1. (A) The preparation process of $\text{Bi}_2\text{Se}_{3-x}/\text{PVDF}$ composite films; and (B) a digital photograph of the flexible $\text{Bi}_2\text{Se}_{3-x}/\text{PVDF}$ films.

The excessive Se in powder is indeterminate and active^[32-34], which is easily oxidized to form selenium oxide during the fabrication of the films, as shown in Equation (2.4).



The phase compositions of the samples were characterized by X-ray diffraction (XRD, Bruker D8 four-circle diffractometer) using $\text{Cu-K}\alpha$ radiation. The morphology and element content of the samples were analyzed by scanning electron microscope (SEM, ZEISS SIGMA, FEI-Siron) and inductively coupled plasma mass spectrometry (ICP-MS, Agilent 725ES and Agilent 5110), respectively. The spectra of the elements were obtained by X-ray photoelectron spectroscopy analysis (XPS, Thermo ESCALAB 250XI). The transmission electron microscopy (TEM, FEI/Tecnai G2 F20S-TWIN TMP TEM) technique was adopted to further analyze the microstructures of films.

The electrical conductivity and Seebeck coefficient were measured simultaneously in a helium atmosphere by an MRS-3 measurement system (thermoelectric measurement system, Joule Yacht). The room-temperature Hall carrier concentration and mobility were obtained by a Hall measurement (HMS-7000).

RESULTS AND DISCUSSION

Characterization of $\text{Bi}_2\text{Se}_{3-x}/\text{PVDF}$ composite films

XRD measurement of $\text{Bi}_2\text{Se}_{3-x}/\text{PVDF}$ thermoelectric composite films ($x = 0, 0.2, 0.3, 0.4$) was performed, as shown in Figure 2A and B. The diffraction peaks are consistent with the standard Bi_2Se_3 card (PDF #33-0214), indicating that the main crystal phase is Bi_2Se_3 . For these composite films, the three main diffraction peaks are (015), (006), and (1,0,10), where (015) possesses the highest intensity among all these peaks, indicating that most Bi_2Se_3 grains grow along the (015) direction. It should be noted that the phase structures are not changed due to the increasing Se content in the films. Additionally, some diffraction peaks of the SeO_3 phase can also be observed at $\sim 26.7^\circ$, although they are not found in the powder

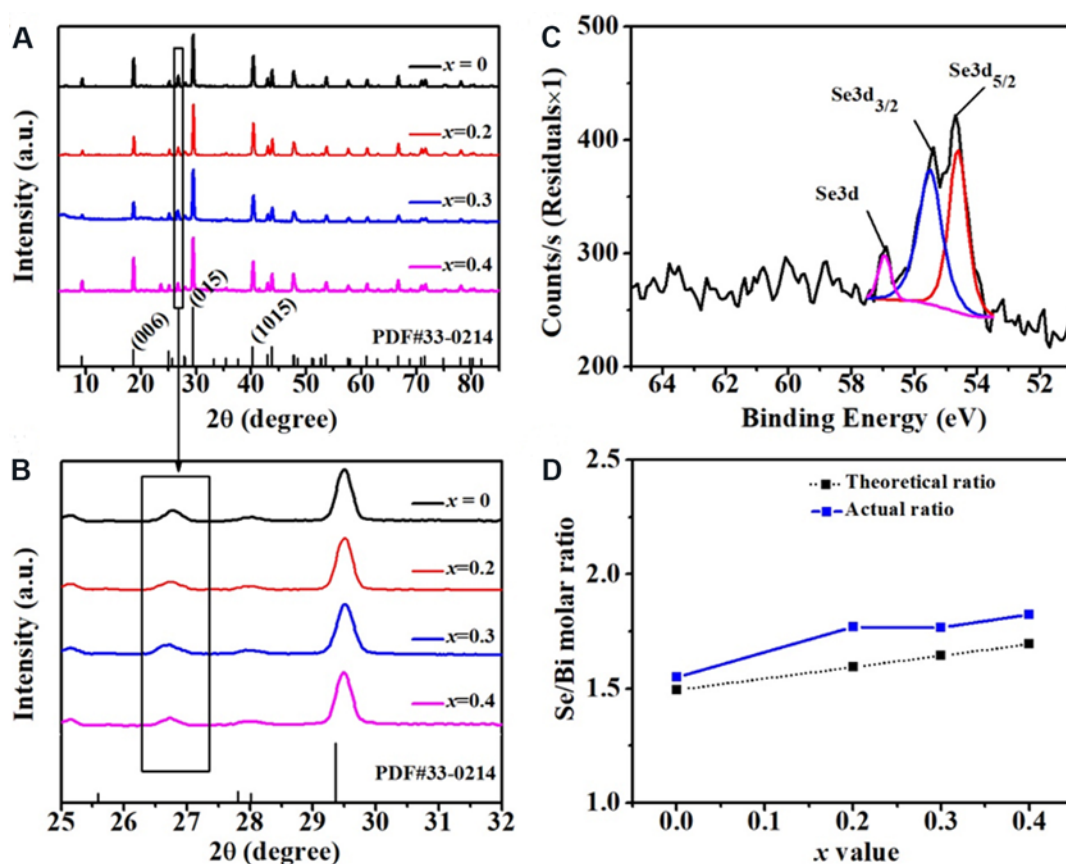


Figure 2. (A, B) XRD patterns of the $\text{Bi}_2\text{Se}_{3+x}$ /PVDF composite films; (C) XPS spectra fitting curve for $\text{Bi}_2\text{Se}_{3.2}$ powder; and (D) Se/Bi molar ratio of ICP-MS measurement for $\text{Bi}_2\text{Se}_{3+x}$ ($x = 0, 0.2, 0.3, 0.4$) powder.

samples [Supplementary Figure 1]. Figure 2C shows the XPS spectrum of $\text{Bi}_2\text{Se}_{3.2}$ powder, which is in good agreement with the standard binding energy cards. The two prominent peaks at 54.63 and 55.51 eV correspond to $\text{Se}3d_{5/2}$ and $\text{Se}3d_{3/2}$, respectively, which indicates the existence of Se^{2-} in the films. Besides, there is a peak with low intensity at 56.95 eV [Figure 2C, Supplementary Table 1], which can be attributed to the elemental Se. Combining with the results of XRD and XPS, we can conclude that there is some Se in the synthesized $\text{Bi}_2\text{Se}_{3+x}$ powder, which is easy to be oxidized in the fabrication process of $\text{Bi}_2\text{Se}_{3+x}$ /PVDF composite films due to the high reactivity, eventually resulting in the formation of SeO_3 .

We also analyzed the element content in the $\text{Bi}_2\text{Se}_{3+x}$ ($x = 0, 0.2, 0.3, 0.4$) samples by ICP-MS, as shown in Figure 2D. As x increases, the measured Se/Bi values are slightly higher than the theoretical values, although they show a consistent changing trend. The reasons can be attributed to the following two aspects: (1) according to the results of XRD and XPS, there is some Se in the $\text{Bi}_2\text{Se}_{3+x}$ powder, which did not react with Bi ions; and (2) the unreacted Bi ions are removed in the process of precipitation $\text{Bi}_2\text{Se}_{3+x}$ powder, resulting in the decreasing Bi content in the materials [Supplementary Figure 2].

Figure 3A and Supplementary Figure 3 show the surface morphology of composite films. All the composite films are formed by hexagonal sheets, which are connected by PVDF. By adjusting the $\text{Bi}_2\text{Se}_{3+x}$ /PVDF:DMF ratio and the solution volume dripped on the glass substrates, composite films with different thicknesses can be prepared. Figure 3B shows the thickness of the $\text{Bi}_2\text{Se}_{3.2}$ /PVDF composite films, around 28.83 μm . The TEM technique was adopted to further analyze the microstructures, as shown in Figure 3C-E. The Bi_2Se_3 hexagonal sheet was obviously observed [Figure 3C], consistent with the results of SEM. Figure 3D

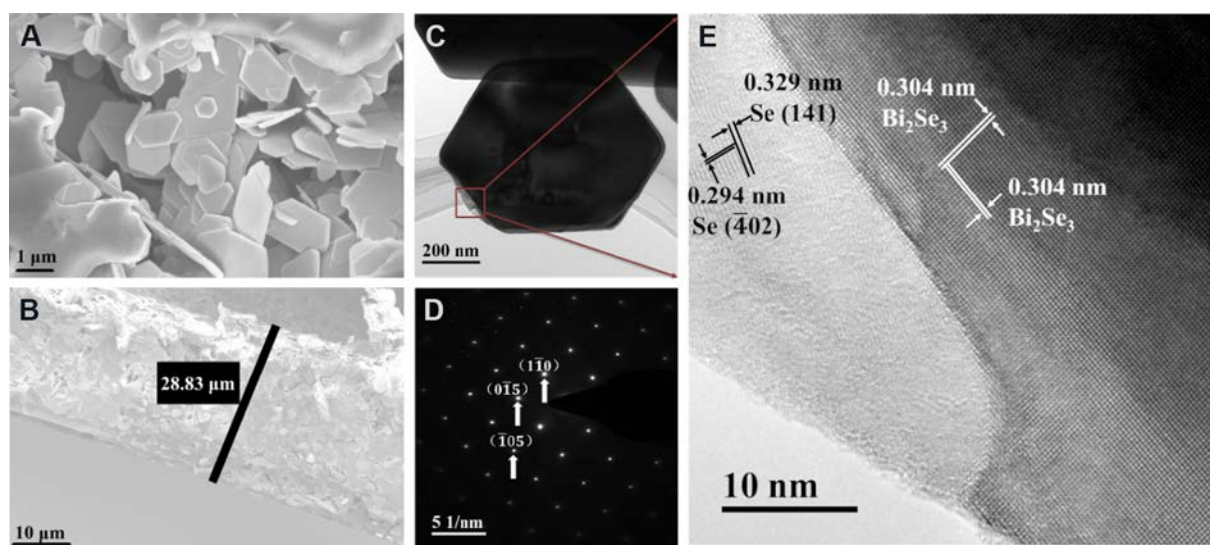


Figure 3. (A, B) Surface and cross-section SEM image of $\text{Bi}_2\text{Se}_{3.2}/\text{PVDF}$ composite films; and (C-E) in-plane TEM image, HRTEM image of the region in (C), and the SAED corresponding to the main phase.

is the HRTEM image of the region in [Figure 3C](#), where the measured lattice spacing values are 0.304 nm, corresponding to (015) and ($\bar{1}05$) crystal planes of Bi_2Se_3 , respectively. It should be noted that it is challenging to distinguish specific crystal plane [i.e., (015) or ($\bar{1}05$)] due to the same lattice spacing. The selected area electron diffraction (SAED) further verifies the crystal structure of Bi_2Se_3 [[Figure 3E](#)]. However, the Se phase can also be observed, which has a different crystal structure and is separated from Bi_2Se_3 . The lattice spacing values of the Se crystals are 0.294 and 0.329 nm, which correspond to the ($\bar{4}02$) and (141) crystal planes, respectively. In this case, the $\text{Bi}_2\text{Se}_3/\text{Se}$ heterostructure is formed. Furthermore, there are many heterostructure interfaces between Bi_2Se_3 nanosheets and PVDF, all of which can adjust the carrier transportation, leading to the improved thermoelectric performance of the films. Additionally, the amorphous material shown in [Figure 3D](#) is primarily caused by the bombardment of the high-speed moving electron beam in the TEM measurement.

Thermoelectric performance of $\text{Bi}_2\text{Se}_{3+x}/\text{PVDF}$ composite films

For the $\text{Bi}_2\text{Se}_{3+x}/\text{PVDF}$ composite films, the temperature-dependent thermoelectric performance is demonstrated in [Figure 4](#). [Figure 4A](#) shows the negative values of the Seebeck coefficient, indicating n-type conduction behavior. With the increasing temperature up to 300 K, the Seebeck coefficient increases slightly. Then, as the temperature further increases, the value of the Seebeck coefficient decreases. Furthermore, the Seebeck coefficient firstly increases and then decreases with the increasing Se concentration. Theoretically, the Seebeck coefficient depends on the carrier concentration and the scattering mechanism^[28,31,35,36].

$$S = \frac{8\pi^2 \kappa_B^2}{3eh^2} \cdot m^* T \left(\frac{\pi}{3n}\right)^{2/3} \quad (3.1)$$

where e is the carrier charge, n is the carrier concentration, μ is the carrier mobility, κ_B is the Boltzmann constant, h is Planck's constant, and m^* is the effective mass of the charge carrier. To further analyze the changing thermoelectric parameters, Hall measurement was performed, as shown in [Figure 4D](#) and [Table 1](#). As can be seen, compared with the undoped sample, the carrier concentrations of samples increased when extra Se was added, which explains the decreasing Seebeck coefficient. For the $\text{Bi}_2\text{Se}_{3+x}/\text{PVDF}$ ($x = 0, 0.2, 0.3, 0.4$) composite films, the room temperature values of Seebeck coefficient are -182.7, -153.0, -163.0, and -170.7 $\mu\text{V}/\text{K}$, respectively.

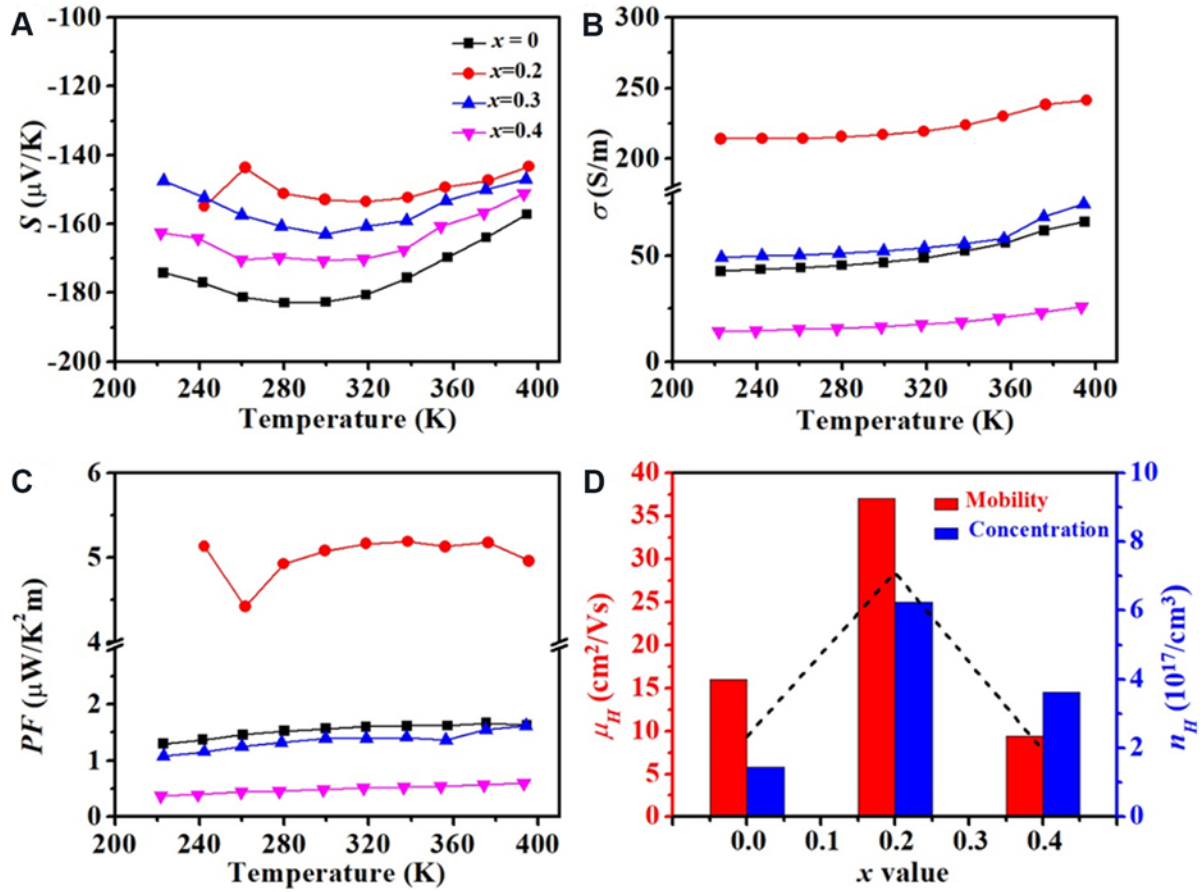


Figure 4. Temperature-dependent thermoelectric properties of $\text{Bi}_2\text{Se}_{3+x}/\text{PVDF}$ composite films: (A) Seebeck coefficient; (B) electrical conductivity; (C) power factor; and (D) Hall carrier concentration and mobility at room temperature.

Table 1. Hall measurement data of $\text{Bi}_2\text{Se}_{3+x}/\text{PVDF}$ composite films at room temperature

Composition	Hall coefficient (cm^3/C)	Mobility (cm^2/Vs)	Carrier concentration ($10^{17}/\text{cm}^3$)
$\text{Bi}_2\text{Se}_3/\text{PVDF}$ film	-42.96	16.02	1.45
$\text{Bi}_2\text{Se}_{3.2}/\text{PVDF}$ film	-10.03	37.07	6.23
$\text{Bi}_2\text{Se}_{3.4}/\text{PVDF}$ film	-17.23	9.39	3.63

The electrical conductivities dependent on temperature are shown in Figure 4B. With the increasing temperature, the electrical conductivities of $\text{Bi}_2\text{Se}_{3+x}/\text{PVDF}$ composite films increase, indicating the semiconductor conduction behavior. Furthermore, as the Se content increases, the electrical conductivities first increase and then decrease, which reaches the highest values when $x = 0.2$, about 216.9 S/m at 300 K. It is well known that the electrical conductivity is determined by the carrier concentration and mobility, as expressed by the following equation:

$$\sigma = en\mu \quad (3.2)$$

Obviously, compared with the composite films without adding extra Se, the carrier concentration and mobility of the $\text{Bi}_2\text{Se}_{3.2}/\text{PVDF}$ composite films are enhanced [Figure 4D, Table 1], which are $\sim 6.23 \times 10^{17}/\text{cm}^3$ and $\sim 37.07 \text{ cm}^2/\text{Vs}$, respectively, leading to the improved electrical conductivity. However, as the Se content further increases, both the carrier concentration and mobility are reduced, which may be due to the impurities (e.g., SeO_3) and the increasing heterostructure interfaces. At room temperature, the electrical conductivities of $\text{Bi}_2\text{Se}_{3+x}/\text{PVDF}$ composite films are ~ 46.9 , ~ 217.0 , ~ 52.2 , and ~ 16.5 S/m, respectively, when $x = 0, 0.2, 0.3$, and 0.4 .

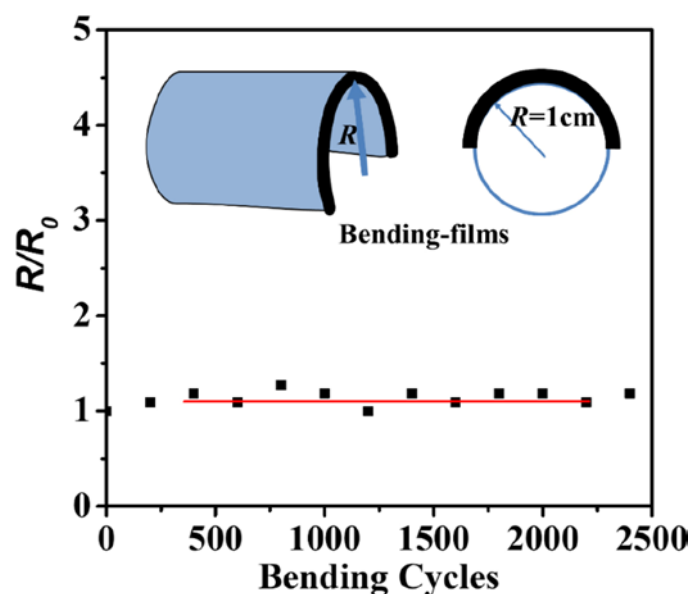


Figure 5. Mechanical stability test of $\text{Bi}_2\text{Se}_{3.2}/\text{PVDF}$ composite films.

The power factor of $\text{Bi}_2\text{Se}_{3+x}/\text{PVDF}$ composite films was calculated based on the above-discussed Seebeck coefficient and electrical conductivity, as shown in Figure 4C. The power factor first increases, then reaches the peak value, and finally decreases with the increasing Se content. Doping with a small amount of Se element ($x \leq 0.2$) increases the electrical conductivity and Seebeck coefficient. When $x = 0.2$, the composite films possess the highest power factor among all films, up to $5.2 \mu\text{W}/\text{K}^2\text{m}$ at 300 K, increasing by ~ 3 times compared with the original sample ($x = 0$). After further doping with Se element ($x > 0.2$), it reduces. This suggests that introducing a small amount of Se into matrix materials is an effective strategy to improve the thermoelectric performance of $\text{Bi}_2\text{Se}_{3+x}/\text{PVDF}$ composite films. It should be noted that the power factor is lower than that of some reports^[29], which mainly results from the poor vacuum of the reacting device.

Mechanical stability of $\text{Bi}_2\text{Se}_{3+x}/\text{PVDF}$ composite films

$\text{Bi}_2\text{Se}_{3.2}/\text{PVDF}$ composite thermoelectric films with a dimension of $2.6 \text{ cm}^2 \times 7.6 \text{ cm}^2$ were chosen to evaluate the material flexibility. Figure 5 shows the film resistance dependent on the bending cycles at a bending radius of 1 cm. R_0 and R represent the initial values and measured values of the resistance, respectively. It can be seen that, after 2500 bending cycles, the R/R_0 value of the sample remains almost constant, indicating the good flexibility. This mainly results from the organic PVDF, which can buffer the deformation and protect the matrix materials from destruction, suggesting that $\text{Bi}_2\text{Se}_{3+x}/\text{PVDF}$ composite thermoelectric films have potential for dynamic applications.

CONCLUSION

Flexible $\text{Bi}_2\text{Se}_{3+x}/\text{PVDF}$ composite films were successfully fabricated by the facile chemical solution method, where the hexagonal Bi_2Se_3 nanosheets were connected by PVDF. By adjusting the content of Se in the raw material, the carrier concentration and mobility were effectively adjusted, leading to improved thermoelectric properties. Compared with the sample without Se element doping, the optimized power factor of $\text{Bi}_2\text{Se}_{3.2}/\text{PVDF}$ composite film is $5.2 \mu\text{W}/\text{K}^2\text{m}$ at 300 K, which is increased by nearly three times. Furthermore, there is no degradation in performance for the composite films after 2500 bending cycles at a radius of 1 cm, showing the good flexibility and mechanical stability.

DECLARATIONS

Authors' contributions

Made substantial contributions to conception: Zou Q, Shang H, Ding F

Design of the study: Zou Q, Shang H, Ding F

Data analysis and interpretation: Qi Zou, Shang H, Huang D, Li T, Xie B

Data acquisition: Qi Zou

Administrative, technical, and material support: Gu H, Ding F

Manuscript writing: Qi Zou, Shang H

Availability of data and materials

Not applicable.

Financial support and sponsorship

This work was supported by the National Natural Science Foundation of China (Grant No. U1832131, Grant No 52072366, Grant No U2032217, and Grant No. 51721005), the Beijing Natural Science Foundation (Grant No. 3202034), and the Youth Innovation Promotion Association of the Chinese Academy of Sciences (Y202041).

Conflicts of interest

All authors declared that there are no conflicts of interest.

Ethical approval and consent to participate

Not applicable.

Consent for publication

Not applicable.

Copyright

© The Author(s) 2021.

REFERENCES

1. Yang J, Liu Q, Deng Z, et al. Ionic liquid-activated wearable electronics. *Materials Today Physics* 2019;8:78-85.
2. Gao M, Li L, Song Y. Inkjet printing wearable electronic devices. *J Mater Chem C* 2017;5:2971-93.
3. Nozariasbmarz A, Collins H, Dsouza K, et al. Review of wearable thermoelectric energy harvesting: from body temperature to electronic systems. *Applied Energy* 2020;258:114069.
4. Zhang Y, Park SJ. Flexible organic thermoelectric materials and devices for wearable green energy harvesting. *Polymers (Basel)* 2019;11:909.
5. Wang Y, Yang L, Shi XL, et al. Flexible thermoelectric materials and generators: challenges and innovations. *Adv Mater* 2019;31:e1807916.
6. Jung YS, Jeong DH, Kang SB, et al. Wearable solar thermoelectric generator driven by unprecedentedly high temperature difference. *Nano Energy* 2017;40:663-72.
7. Chang C, Zhao L. Anharmonicity and low thermal conductivity in thermoelectrics. *Materials Today Physics* 2018;4:50-7.
8. Kang SD, Pöhls J, Aydemir U, et al. Enhanced stability and thermoelectric figure-of-merit in copper selenide by lithium doping. *Materials Today Physics* 2017;1:7-13.
9. Zhai R, Wu Y, Zhu T, Zhao X. Thermoelectric performance of p-type zone-melted Se-doped Bi_{0.5}Sb_{1.5}Te₃ alloys. *Rare Met* 2018;37:308-15.
10. Guan M, Qiu P, Song Q, et al. Improved electrical transport properties and optimized thermoelectric figure of merit in lithium-doped copper sulfides. *Rare Met* 2018;37:282-9.
11. He R, Zhu H, Sun J, et al. Improved thermoelectric performance of n-type half-Heusler MCo_{1-x}Ni_xSb (M = Hf, Zr). *Materials Today Physics* 2017;1:24-30.
12. Ding Y, Qiu Y, Cai K, et al. High performance n-type Ag₂Se film on nylon membrane for flexible thermoelectric power generator. *Nat Commun* 2019;10:841.
13. Liu R, Tan X, Liu Y, et al. BiCuSeO as state-of-the-art thermoelectric materials for energy conversion: from thin films to bulks. *Rare Met* 2018;37:259-73.

14. Wu Y, Li W, Faghaninia A, et al. Promising thermoelectric performance in van der Waals layered SnSe₂. *Materials Today Physics* 2017;3:127-36.
15. Ma S, Li C, Wei P, et al. High-pressure synthesis and excellent thermoelectric performance of Ni/BiTeSe magnetic nanocomposites. *J Mater Chem A* 2020;8:4816-26.
16. Cecchi S, Dragoni D, Kriegner D, et al. Interplay between structural and thermoelectric properties in epitaxial Sb_{2-x}Te₃ alloys. *Adv Funct Mater* 2019;29:1805184.
17. Chen Y, Fan Z, Zhang Z, et al. Two-dimensional metal nanomaterials: synthesis, properties, and applications. *Chem Rev* 2018;118:6409-55.
18. Atwa M, Nakagawa T, Yonamine A, et al. Top-down approach using supercritical carbon dioxide ball milling for producing sub-10 nm Bi₂Te₃ grains. *Appl Phys Express* 2020;13:067002.
19. Ambrosi A, Sofer Z, Luxa J, Pumera M. Exfoliation of layered topological insulators Bi₂Se₃ and Bi₂Te₃ via electrochemistry. *ACS Nano* 2016;10:11442-8.
20. Zhao M, Huang Y, Peng Y, Huang Z, Ma Q, Zhang H. Two-dimensional metal-organic framework nanosheets: synthesis and applications. *Chem Soc Rev* 2018;47:6267-95.
21. Gui R, Jin H, Sun Y, Jiang X, Sun Z. Two-dimensional group-VA nanomaterials beyond black phosphorus: synthetic methods, properties, functional nanostructures and applications. *J Mater Chem A* 2019;7:25712-71.
22. Liu J, Wang H, Li X, et al. High performance visible photodetectors based on thin two-dimensional Bi₂Te₃ nanoplates. *J Alloys Compd* 2019;798:656-64.
23. Shang H, Ding F, Li G, et al. High performance co-sputtered Bi₂Te₃ thin films with preferred orientation induced by MgO substrates. *J Alloys Compd* 2017;726:532-7.
24. Shang H, Dun C, Deng Y, et al. Bi_{0.5}Sb_{1.5}Te₃-based films for flexible thermoelectric devices. *J Mater Chem A* 2020;8:4552-61.
25. Yoo T, Lee E, Dong S, et al. Thermal conductivity of Bi₂(Se_xTe_{1-x})₃ alloy films grown by molecular beam epitaxy. *APL Materials* 2017;5:066101.
26. Wudil Y, Gondal M, Rao S, Kunwar S. Thermal conductivity of PLD-grown thermoelectric Bi₂Te_{2.7}Se_{0.3} films using temperature-dependent Raman spectroscopy technique. *Ceramics International* 2020;46:7253-8.
27. Liu W, Jie Q, Kim HS, Ren Z. Current progress and future challenges in thermoelectric power generation: from materials to devices. *Acta Materialia* 2015;87:357-76.
28. Masood KB, Farooq U, Singh J. Evolution of the structural, dielectric and electrical transport properties of Bi₂Te₃ nano-sticks synthesized via polyol and solvothermal routes. *Physica B Condensed Matter* 2020;588:412183.
29. Dun C, Hewitt CA, Huang H, et al. Layered Bi₂Se₃ nanoplate/polyvinylidene fluoride composite based n-type thermoelectric fabrics. *ACS Appl Mater Interfaces* 2015;7:7054-9.
30. Chen X, Feng L, Yu P, et al. Flexible thermoelectric films based on Bi₂Te₃ nanosheets and carbon nanotube network with high n-type performance. *ACS Appl Mater Interfaces* 2021;13:5451-9.
31. Li S, Liu Y, Liu F, et al. Effective atomic interface engineering in Bi₂Te_{2.7}Se_{0.3} thermoelectric material by atomic-layer-deposition approach. *Nano Energy* 2018;49:257-66.
32. Kong D, Cha JJ, Lai K, et al. Rapid surface oxidation as a source of surface degradation factor for Bi₂Se₃. *ACS Nano* 2011;5:4698-703.
33. Zhang L, Yang H, Yu J, et al. Controlled synthesis and photocatalytic activity of ZnSe nanostructured assemblies with different morphologies and crystalline phases. *J Phys Chem C* 2009;113:5434-43.
34. Zhou B, Zhu JJ. Microwave-assisted synthesis of Sb₂Se₃ submicron rods, compared with those of Bi₂Te₃ and Sb₂Te₃. *Nanotechnology* 2009;20:085604.
35. Liu S, Peng N, Bai Y, Ma D, Ma F, Xu K. Fabrication of Cu-Doped Bi₂Te₃ nanoplates and their thermoelectric properties. *Journal of Elec Materi* 2017;46:2697-704.
36. Cam Tuyen LT, Le PH, Luo CW, Leu J. Thermoelectric properties of nanocrystalline Bi₃Se₂Te thin films grown using pulsed laser deposition. *J Alloys Compd* 2016;673:107-14.